bjh research paper

Estimation of dose requirements for sustained *in vivo* activity of a therapeutic human anti-CD20 antibody

Wim K. Bleeker,[1] Martin E. Munk,[2] Wendy J. M. Mackus,[1] Jeroen H. N. van den Brakel,[1] Marielle Pluyter,[1] Martin J. Glennie,[3] Jan G. J. van de Winkel[1,4] and Paul W. H. I. Parren[1]

[1]Genmab, Utrecht, The Netherlands, [2]Genmab, Copenhagen, Denmark, [3]Tenovus Research Laboratory, Cancer Sciences Division, School of Medicine, University General Hospital, Southampton, UK, and [4]Immunotherapy Laboratory, Department of Immunology, University Medical Centre, Utrecht, The Netherlands

Received 27 June 2007; accepted for publication 18 September 2007

Correspondence: Paul W. H. I. Parren, Research and Technology, Genmab B.V., Yalelaan 60, 3584 CM Utrecht, The Netherlands.
E-mail: p.parren@genmab.com

Summary

We evaluated the dose requirements for sustained *in vivo* activity of ofatumumab, a human anti-CD20 antibody under development for the treatment of B cell-mediated diseases. In a mouse xenograft model, a single dose, resulting in an initial plasma antibody concentration of 5 μg/ml, which was expected to result in full target saturation, effectively inhibited human B-cell tumour development. Tumour growth resumed when plasma concentrations dropped below levels that are expected to result in half-maximal saturation. Notably, tumour load significantly impacted antibody pharmacokinetics. In monkeys, initial depletion of circulating and tissue residing B cells required relatively high-dose levels. Re-population of B-cell compartments, however, only became detectable when ofatumumab levels dropped below 10 μg/ml. We conclude that, once saturation of CD20 throughout the body has been reached by high initial dosing, plasma concentrations that maintain target saturation on circulating cells (5–10 μg/ml) are probably sufficient for sustained biological activity. These observations may provide a rationale for establishing dosing schedules for maintenance immunotherapy following initial depletion of CD20 positive (tumour) cells.

Keywords: antibody therapy, B cells, leukaemia, animal model.

In the last decade, therapeutic monoclonal antibodies (mAb) have been established as a rapidly expanding class of drugs, especially since the development of humanized and fully human mAb (Glennie & van de Winkel, 2003; Carter, 2006). The 20 mAbs currently approved by the Food and Drug Administration are used for widely varying clinical conditions: transplant rejection, cancer, rheumatoid arthritis and preventing viral infection. A number of therapeutic antibodies are currently well established in the treatment of haematological malignancies. Notably, the chimaeric anti-CD20 mAb, rituximab, is successful in the therapy of B-lymphoid malignancies and rheumatoid arthritis (Grillo-Lopez *et al*, 2000; De Vita & Quartuccio, 2006).

Antibodies may exert their therapeutic effects in different ways (Glennie, 2000). Previously, we have reported the *in vitro* characterization of a new panel of human antibodies against CD20, which were generated using human immunoglobulin transgenic mice (Teeling *et al*, 2004, 2006). These studies showed marked differences between anti-CD20 antibodies with respect to the therapeutic effector mechanisms involved in the killing of CD20 positive tumour cells. All tested anti-CD20 human mAb were able to induce antibody-dependent cellular cytotoxicity (ADCC) with human effector cells derived from peripheral blood. However, two mAb, 2F2 (ofatumumab) and 7D8, were remarkably active in complement-dependent cytotoxicity (CDC), being able to lyse low CD20-expressing chronic lymphocytic leukaemia (CLL) cells in the presence of human plasma or unfractionated peripheral blood. Ofatumumab (HuMax-CD20) was selected for further clinical development.

An important parameter for the therapeutic application of mAb is the minimal dose required for full *in vivo* efficacy. Generally speaking, the dose–effect relationships for a therapeutic antibody are expected to correspond to the binding curve of the antibody to the target. However, there may be differences in the required occupancy of the target, depending on the underlying therapeutic mechanism. For example, engagement of immune-effector functions is expected to require a certain number of antibodies in the proper arrangement on a cell membrane for effective interaction with either

First published online 28 November 2007

soluble C1q or Fc receptors present on effector cells. Maximum engagement of soluble or cell-bound ligands may already occur before maximal antibody binding is achieved. Furthermore, the pharmacokinetics of the antibody needs to be understood for a rational determination of the optimal-dosing schedule.

This study addressed the issue of optimal dosing of ofatumumab in an *in vivo* mouse tumour xenograft model with a luciferase-transfected human B-cell line, in which tumour development was monitored by bioluminescence imaging. Furthermore, we studied ofatumumab-induced B-cell depletion and recovery in healthy cynomolgus monkeys. This study resulted in an estimation of the minimal effective plasma concentration in experimental animal models, and better understanding of the pharmacokinetic profile of the antibody.

Materials and methods

Antibodies

Human IgG1 kappa antihuman-CD20 mAbs were generated by immunizing human immunoglobulin transgenic HCo7 and KM mice (Fishwild *et al*, 1996) with human CD20-expressing NS/0 cells. Antibody 2F2 (Ofatumumab, HuMax-CD20; IgG1, κ; Genmab, Utrecht, the Netherlands) was selected from a panel of several mAbs for its potent engagement of immune-effector mechanisms, particularly the induction of CDC on CD20 expressing cells (Teeling *et al*, 2004). A human IgG1 kappa, specific for keyhole limpet haemocyanin (KLH) was developed using the same technique and served as isotype IgG control. The antibodies were purified by protein A affinity chromatography, followed by size exclusion chromatography.

In vitro cytotoxicity assays

The capacity of mAb to induce ADCC and CDC of tumour cells was evaluated in Chromium-51 (^{51}Cr) release assays using Daudi cells [American Type Culture Collection, (ATCC), Manassas, VA, USA], a CD20-expressing B-cell line originating from Burkitt lymphoma, as target cells.

Daudi cells were cultured in RPMI culture medium (RPMI 1640, Bio Whittaker, Walkersville, ND, USA) supplemented with 10% bovine calf serum (Cosmic Calf Serum, Hyclone, Logan, UT, USA), Pen/ Strep, L-Glutamine and Na-Pyruvate. Cells ($2–5 \times 10^6$) were labelled with 3·7 MBq $Na_2{}^{51}CrO_4$ (Amersham Biosciences, Uppsala, Sweden) under shaking conditions at 37°C for 1 h. Labelled cells in culture medium were dispensed in 96-wells plates (5×10^3/well) and pre-incubated for 15 min with threefold serial dilutions of ofatumumab, at concentrations ranging from 100 μg/ml to 0·5 ng/ml.

Human peripheral blood monouclear cells (PBMC) were isolated from buffy coats from standard blood donations (Sanquin Blood Bank, Utrecht, the Netherlands) using density separation on Lymphocyte Separation Medium (Lymphoprep; Bio Whittaker). After centrifugation, PBMC were collected and washed with RPMI culture medium (Bio Whittaker) until the supernatant was clear.

For measuring CDC induction, fresh-frozen human pool serum was added to a final volume of 20% (v/v) and the plates were incubated for 1 h at 37°C. For determining ADCC induction, human peripheral blood mononuclear cells (PBMC) were added in a 100:1 ratio and the plates were incubated for 4 h at 37°C. Target cells were incubated in medium without antibodies, serum or effector cells to determine the spontaneous ^{51}Cr release; triton ×100 (1% final concentration) was added to determine the maximal ^{51}Cr release. Plates were centrifuged before collecting supernatant for measuring ^{51}Cr release with a gamma counter (Cobra; Packard-PerkinElmer, Brussels, Belgium). Percentage of specific cell lysis was calculated using the following formula:

% specific lysis = [experimental release (cpm) – spontaneous release (cpm)]/[maximal release (cpm) – spontaneous release (cpm)] × 100%.

Luciferase-transfected Daudi cells

Daudi cells were transfected by electroporation with gWIZ luciferase (Aldevron, Fargo, ND, USA) and pPur vector (BD Biosciences, Alphen a/d Rijn, The Netherlands) in a 4:1 ratio and, after 48 h, puromycin was added for selecting a stably transfected clone (Daudi-luc).

Mouse xenograft model

Female severe combined immunodeficient (SCID) mice (C.B-17/IcrCrl-scid-BR, Charles River, Maastricht, the Netherlands), 8–10 weeks old, were housed in a barrier unit in sterile filter-top cages. Sterile food and water were provided *ad libitum*. All mouse experiments were approved by the Animal Ethics Committee of the University of Utrecht.

Tumour xenografts were induced by injecting $2·5 \times 10^6$ Daudi-luc cells into the tail vein. At a predetermined time point, groups of mice were treated with single i.p. doses of either ofatumumab or the anti-KLH control mAb, in a blinded fashion. At least twice weekly, mice were checked for clinical signs. At weekly intervals, tumour growth was assessed using bioluminescence imaging of the back view of the mice. Before imaging mice were anaesthetized by i.p. injection of a mix of ketamine/xylazine/atropine. Synthetic D-luciferin (Biothema, Handen, Sweden) was given i.p. at a dose of 125 mg/kg. Mice were then placed backside up, in a light box and 10 min after luciferin administration, imaging was started using a VersArray 1300B CCCD camera (Roper Scientific, Vianen, the Netherlands). Light was detected in a photon-counting manner over an exposure period of 5 min. Under illumination, black and white images were made for anatomical reference. METAVUE software (Universal Imaging Corp., Downingtown, PA, USA) was used for data collection and image analysis. During the study, two heparinized blood samples were taken

from the orbital plexus. The experiment was ended at 6–8 weeks after initiation of treatment, depending on imaging results. If mice showed clinical signs that could be related to tumour development, such as hind leg paralysis, the treatment group concerned was ended prematurely for ethical reasons.

A separate series with three tumour-free mice was performed to determine the plasma clearance of ofatumumab in more detail. In this experiment, ofatumumab was given as a single i.p. dose of 5 mg/kg and blood samples were collected after 5 h, 1, 2, 4, 7, 21 and 28 d.

Non-human primate model

Studies in cynomolgus monkeys (*Macaca fascicularis*) were performed to establish the pharmacokinetic and toxicological profiles of ofatumumab at different dose levels. CD20 is strongly conserved between humans and cynomolgus monkeys, with only one amino acid difference in the extracellular loops. The affinity of ofatumumab for human and monkey was determined to be similar and target saturation therefore occurred at similar antibody concentrations (half maximal effective concentration [EC50]: 0·28 and 0·14 μg/ml for human and monkey, respectively). The studies were conducted at Charles River Laboratories (Tranent, UK) in accordance with the European Convention for the Protection of Vertebrate Animals Used for Experimental and Other Scientific Purposes (Council of Europe), under control of the UK Home Office. Monkeys, weighing 2·2–2·8 kg, were obtained from Charles River (Houston, TX, USA). Three male and three female cynomolgus monkeys were assigned to three dose groups, receiving ofatumumab at dose levels of 1·25, 6·25 and 12·5 mg/kg, once daily as i.v. (30 min) infusions for four consecutive days. In a second study, cynomolgus monkeys received weekly administrations of ofatumumab for 4 weeks (20 or 100 mg/kg). All animals were observed at least twice daily for signs of ill health or reaction to treatment. Blood samples for laboratory investigations [haematology, coagulation, clinical chemistry, primate antihuman antibody (PAHA) measurements and flow cytometry] were collected from the femoral vein throughout the dosing and postdose observation periods. Lymph node biopsies were obtained (from the superficial lymph nodes) throughout the study period. On completion of the postdose observation period, the animals were sacrificed and subjected to a detailed necropsy. Organs and tissues were weighed and subjected to histological evaluation. Selected tissues were also stained for immunohistochemical investigations.

Analysis of serum antibodies

Ofatumumab plasma levels in mice were determined using an enzyme-linked immunosorbent assay (ELISA) for human IgG in which mouse antihuman IgG1 mAb MH16-1 (CLB/Sanquin, Amsterdam, the Netherlands) was used to coat 96-well Microlon ELISA plates (Greiner, Frickenhausen, Germany). After blocking plates with ELISA buffer [phosphate-buffered saline (PBS) supplemented with 0·05% Tween 20 and 2% chicken serum], samples, serially diluted in ELISA buffer, were added and incubated for 1 h at room temperature. Plates were subsequently incubated with peroxidase labelled goat antihuman IgG Fc-specific immunoglobulin (Jackson, West Grace, PA, USA) and developed with 2,2′-azino-bis (3-ethylbenzthiazoline-6-sulfonic acid) (ABTS; Roche Diagnostics, Mannheim, Germany). The reaction was stopped by adding 0·5 mol/l oxalic acid. Absorbance was measured in a microplate reader (Biotek, Winooski, VT, USA) at 405 nm. Results are expressed in μg/ml, using ofatumumab as reference.

Ofatumumab serum concentrations in monkeys were determined using an ELISA for human IgG in which monkey-preabsorbed sheep antihuman IgG (AF003-M, The Binding Site, Birmingham, UK) was used for capture and a mouse antihuman IgG (Fc-specific) horseradish peroxidase (HRP) conjugate (MH16-1, CLB, Amsterdam, the Netherlands) for detection. The procedure was similar to that described above. The limit of quantification was 1 μg/ml for ofatumumab in monkey plasma.

PAHA assay

The occurrence of PAHA against ofatumumab was tested in an ELISA in which plates were coated with ofatumumab $F(ab')_2$ fragments. After washing, the plates were incubated with serially diluted serum samples. Bound primate IgG was detected using a mouse antihuman IgG (Fc specific) HRP conjugate (MH16-1; CLB, Amsterdam, the Netherlands). Plates were developed using ABTS and absorbance was read 405 nm. The PAHA titre was determined as the highest dilution giving an absorbance of >0·1 over the background and a fourfold increase over the pretreatment value.

Flow cytometry

Antibody binding to Daudi cells *in vitro* was determined after incubating 100 000 cells in 1 ml of serial dilutions of ofatumumab in PBS supplemented with 0·05% bovine serum albumin and 0·02% sodium azide [fluorescent-activated cell sorting (FACS) buffer] at 4°C. Cells were subsequently stained with fluorescein isothiocyanate (FITC)-conjugated $F(ab')_2$ fragments of goat antihuman Fc (Jackson Immunology, Westgrove, PA, USA) as secondary antibodies. Samples were analysed on a FACSCalibur^{TM} system (BD Biosciences).

Cynomolgus peripheral blood samples were collected into EDTA-containing tubes. Erythrocytes were lysed and remaining cells were incubated at 4°C for 20 min with PC5-conjugated antihuman CD20 mouse mAb, clone B9E9 (Beckman Coulter, Mijdrecht, the Netherlands), or with FITC-conjugated antihuman CD21 mouse mAb, clone BL13 (Beckman Coulter), for identifying the B-cells. Viable cells (10 000) within the lymphocyte gate, defined by forward

versus side scatter, were analysed on a Beckham Coulter flow cytometer EPICS XL-MCL™ (Beckham Coulter, Luton, Bedfordshire, UK). For the generation of absolute counts, Flow Count Fluorospheres (Beckham Coulter) were added to the samples. Cynomolgus peripheral lymph node biopsy material was disaggregated using the Medimachine System (Becton Dickinson, Erembodegem-Aalst, Belgium). After processing, cells were incubated with the different mAb as described above. Results are expressed as percentages of total cell count.

Pharmacokinetic analyses

A double-exponential curve-fit using GRAPHPAD PRISM version 3·02 (Graphpad Software, San Diego, CA, USA) was applied to determine the steady state distribution volume and the elimination half-life of ofatumumab in tumour-free mice after a single i.p. dose.

A different approach was used for the monkey studies, as the multiple dosing prevented the use of a double-exponential curve-fit. The pharmacokinetic analyses were done by simulations in a numerical two-compartment model adapted to IgG kinetics, partly described by Bleeker *et al* (2001). In this two-compartment model, the assumption was made that infused IgG is immediately mixed in the plasma compartment of 40 ml/kg and redistributed by approximately 50% into the interstitial space. For simulations, all IgG transfers and subsequent concentration changes were calculated in small discrete time steps. Deviations in ofatumumab pharmacokinetics from the expected IgG kinetics were assessed by comparing actual measurements with simulated plasma concentrations using pharmacokinetic parameters published by Lin *et al* (1999) for a human mAb against vascular endothelial growth factor (VEGF) in mice and monkeys.

Statistics

Statistical significance of differences between groups was determined by one-way ANOVA with a Newman–Keuls post-test using GRAPHPAD PRISM software.

Results

In vitro concentration–effect relationships

Firstly, we performed a series of *in vitro* experiments to establish how the cytotoxic effects of ofatumumab relate to target occupancy. Figure 1 shows results from a typical experiment, in which the concentration–effect relationships for CDC and ADCC induction by ofatumumab were compared with its binding curve. ADCC induction reached the maximum level (51% cell lysis) at an mAb concentration of about 0·1 μg/ml, at which half-maximal target occupancy was achieved. In contrast, full target saturation was required for obtaining maximal CDC (68% cell lysis). It is important to note that no further increase in ADCC or CDC was observed by increasing the ofatumumab concentration above the level giving binding saturation.

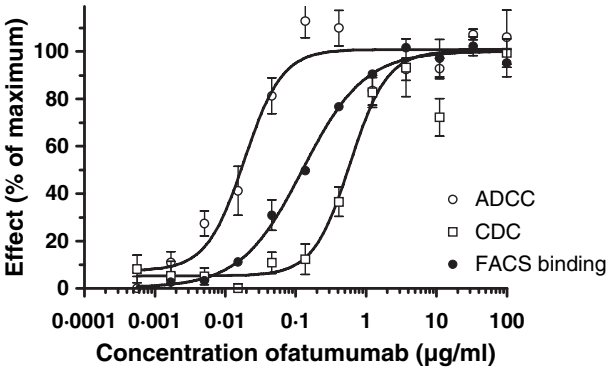

Fig 1. Concentration–effect relationships *in vitro* for ofatumumab regarding antibody-dependent cellular cytotoxicity (ADCC) and complement-dependent cytotoxicity (CDC) induction and binding to Daudi cells. ADCC and CDC induction were determined in ^{51}Cr-release assays; binding to cells was determined using flow cytometry. The effects are expressed as a percentage of the maximum, which were 51% and 68% cell lysis for ADCC and CDC respectively and 1258 mean fluorescence intensity for the FACS assay. Results from a representative experiment are shown; data points are mean and SEM of six replicates for the ADCC and CDC assays and of three replicates for the binding assay. Sigmoidal curves were fit to the data with EC50 values of 0·02, 0·60 and 0·13 μg/ml for ADCC, CDC and FACS binding, respectively.

Mouse tumour xenograft model

To study the *in vivo* dose–effect relationship of ofatumumab, we first analysed ofatumumab in the therapy of established tumour xenografts in SCID mice. Bioluminescence imaging was used for evaluating tumour growth, as it permits the detection of disseminated tumours already at an early stage after which their development can be followed quantitatively in time. Figure 2 shows bioluminescence images made at weekly intervals after i.v. inoculation of luciferase-transfected Daudi B cells (Daudi-luc cells) from an experiment in which an early low-dose treatment was applied. Ofatumumab or control mAb was administered as a single dose of 0·5 mg/kg on day 5 after tumour induction. From day 13 onwards, distinct light-emitting spots were observed in the control mice demonstrating disseminated tumour growth. The light emission steadily increased in the following weeks and the control mice were euthanized on day 35 because clinical signs (significant weight loss) became apparent in two of the mice. This is consistent with other data published on the Daudi xenograft model using the occurrence of clinical signs as endpoint (Cragg & Glennie, 2004). In the ofatumumab-treated mice, tumour growth was also observed, but, in contrast to control mice, only after a delay of 3–4 weeks. Figure 3A shows a plot of the integrated bioluminescence signals in the different groups, as a measure of tumour mass. In a second experiment, shown in Fig 3B, mice were treated at a later stage of tumour

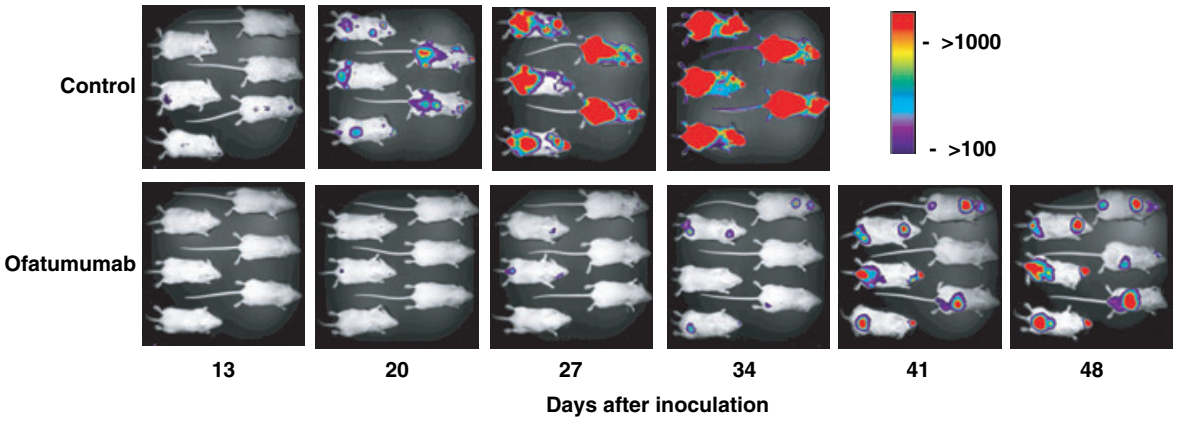

Fig 2. Effect of ofatumumab on *in vivo* tumour development. Bioluminescence imaging was performed at weekly intervals after i.v. inoculation of Daudi-luc cells on day 0. Antibodies were administered on day 5 in a single i.p. dose of 0·5 mg/kg of either ofatumumab (6 mice) or control monoclonal antibodies (6 mice). The images show light emission from the back view of individual mice made at different time points, with the intensity levels represented in pseudo colours ranging from blue (>100) to red (>10 000 U per pixel). For anatomical reference, the light intensities are superimposed on black-and-white pictures of the mice taken under illumination. Experiment is representative for five different experiments, in which ofatumumab was given at different dose levels at different time points after inoculation of Daudi-luc cells.

development with two different dose levels of antibody. Ofatumumab was given as a single dose of either 0·5 or 50 mg/kg on day 14. Treatment with a dose of 50 mg/kg gave significant inhibition of tumour growth, when compared with control treatment, throughout the observation period of 56 d. The low dose of 0·5 mg/kg was equally effective until day 42. On day 56, tumour development in the low-dose group accelerated, compared to that in the high-dose group, suggesting that the protective effect of ofatumumab had ended.

To analyse dose–effect relationships in tumour-bearing mice in more detail, we determined ofatumumab plasma concentrations in xenografted and control SCID mice (Fig 4). Xenografted SCID mice were treated with a single dose of 0·5 mg/kg at 5 or 14 d following tumour induction. In the mice treated 5 d after inoculation of Daudi-luc cells, ofatumumab plasma concentrations remained above 1 μg/ml throughout the experiment (Fig 4A). In the xenografted mice treated 14 d following tumour challenge, the ofatumumab plasma concentration also started above 1 μg/ml, but gradually decreased to values between 0·1 and 0·2 μg/ml near the end of the experiment (Fig 4B). For comparison, the antibody concentrations achieved after i.p. administration of 5 mg/kg of ofatumumab in tumour-free SCID mice ($n = 3$) were plotted (Fig 4C). The antibody distribution volume and half-life in normal SCID mice were determined by applying a double-exponential curve-fitting. A steady state distribution volume of 104 ml/kg and an elimination half-life of 19 ± 0·4 d (mean ± SE) were obtained. This relatively long half-life is normal for human IgG in SCID mice because of the low-total plasma IgG concentrations (Sell & Fahey, 1964). Based on these data, the plasma concentrations that could be expected for a dose of 0·5 mg/kg were estimated, assuming linear kinetics (dashed line, Fig 4). Notably, this showed that the plasma concentrations in the mice treated early following challenge are in accordance with those expected from tumour-free mice. For the mice treated late after tumour induction, the observed values were two to three times below the expected concentrations. This indicated that tumour load may have a profound effect on plasma levels in this model.

Acceleration of tumour growth was observed in this experiment on day 42 after tumour induction. At this time point, ofatumumab plasma concentrations had dropped below 0·4 μg/ml.

Cynomolgus monkey B-cell depletion study

Because the activation of Fc-mediated effector functions appears to play a central role in therapeutic activity of ofatumumab, we next evaluated its dose–response relationship in a non-human primate model. Here, we evaluated *in vivo* activity by examining depletion of monkey B cells in the periphery as well as in lymph nodes. We first focussed on the time course and extent of B-cell depletion and then looked at how this relates to dosing and antibody plasma levels. Figure 5 shows a flow cytometric analysis of $CD20^+$ cells in peripheral blood (Fig 5A) and in lymph nodes (Fig 5B) of animals treated at different i.v. dose levels, 1·25, 6·25 or 12·5 mg/kg daily, administered for four consecutive days (i.e. 5, 12·5 and 50 mg/kg total dose). As two distinct B-cell subsets have been described for cynomolgus monkeys, $CD20^{low}CD40^{high}CD21^+$ and $CD20^{high}CD40^{low}CD21^-$ (Vugmeyster *et al*, 2003), $CD21^+$ cell numbers were also determined. For these cells, equivalent depletion in peripheral blood was observed (data not shown), also indicating that the presence of ofatumumab did not prevent detection of $CD20^+$ cells by flow cytometry. There was an immediate and efficient B-cell depletion at all three dose levels. For the low-dose group (5 mg/kg), $CD20^+$ cell recovery in peripheral blood and in lymph nodes was first detected on

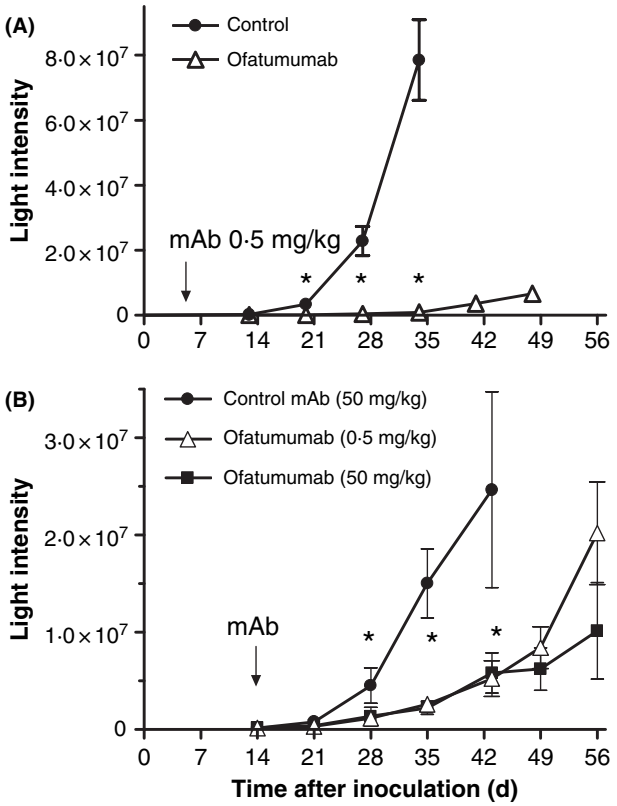

Fig 3. Effectiveness of ofatumumab in relation to dose level in severe combined immunodeficient xenograft model. Bioluminescence imaging was performed at weekly intervals after i.v. inoculation of Daudi-luc cells on day 0. Light emission collected from the back views of mice was integrated over the total body areas of individual mice and plotted in time as measure of tumour mass development. In the series presented in panel A, mice were treated on day 5 with a single 0·5 mg/kg dose of either ofatumumab (open triangles) or anti-keyhole limpet haemocyanin (KLH) control monoclonal antibody (mAb) (solid circles). In the series presented in panel B, mice were treated on day 14 with a single dose of ofatumumab, of either 0·5 mg/kg (open triangles) or 50 mg/kg (solid squares) or with 50 mg/kg of anti-KLH control mAb (solid circles). Control animals were sacrificed for ethical reasons on day 35 or 42. Data represent mean and SEM of six or nine mice per group, in series A and B, respectively. Significant differences between the control group and the ofatumumab-treated groups (ANOVA, $P < 0{\cdot}05$) are indicated by *. The experiment of series B was repeated one time, yielding essentially identical results.

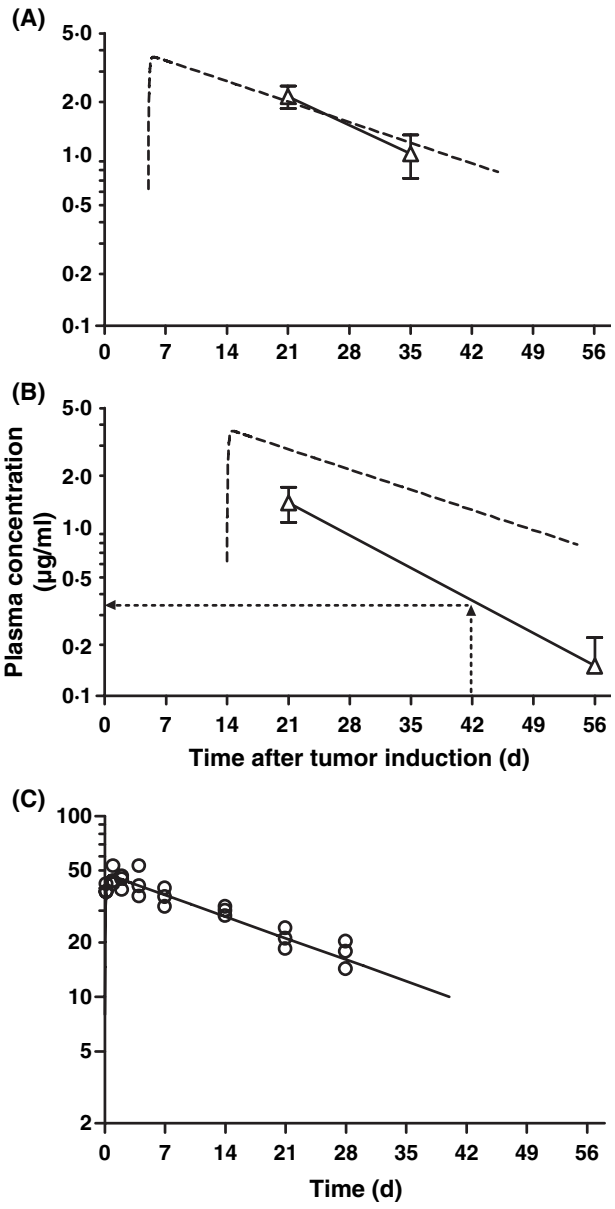

Fig 4. Pharmacokinetic analysis in severe combined immunodeficient mice. Panels A and B relate to the experiments also presented in Fig 3 and show semi-logarithmic plots of ofatumumab plasma concentrations (open triangles, mean and SD) observed in xenografted mice. The dashed lines give the expected plasma concentration profiles, calculated using a linear two-compartment model with the pharmacokinetic parameters derived from Fig 4C. Panel A: single dose of 0·5 mg/kg on day 5 after tumour induction (corresponds to Fig 3A). Panel B: single dose of 0·5 mg/kg on day 14 after tumour induction (corresponds to Fig 3B). The dotted arrows mark the time point at which the ofatumumab in the latter experiment seemed to become ineffective and the corresponding estimated plasma concentration. Panel C: Ofatumumab was administered i.p. into three tumour-free severe combined immunodeficient mice at a dose of 5 mg/kg (open circles) to determine half-life and distribution volume.

day 29 while complete B-cell count recovery (return to pretest cell counts or above) was not observed prior to day 96. After administration of the medium dose (12·5 mg/kg) or high dose (50 mg/kg) of ofatumumab, profound B-cell depletion was observed for at least 56 d. Recovery of B cells to base line levels became apparent 70–90 d after the last dose and was complete at the end of the 136-d observation period. Accordingly, necropsy samples analysed by immunohistochemistry showed full $CD20^+$ cell repopulation in lymph nodes by day 113 (data not shown). The strong B-cell depletion induced by ofatumumab, peripherally and in lymph nodes, was consistent with profound germinal centre atrophy in lymph nodes observed in a parallel experiment in which monkeys were treated for 4 weeks at weekly doses of 20 or 100 mg/kg. Haemotoxylin and Eosin-stained sections of necropsy samples taken 2 weeks after the last dose showed normal lymph node

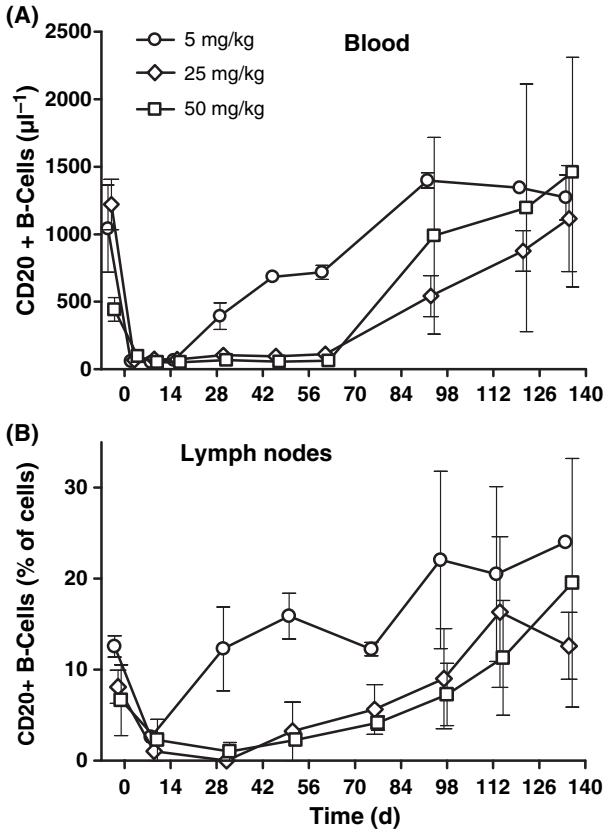

Fig 5. Effect of ofatumumab on peripheral blood and lymph node B-cell levels in monkeys. Ofatumumab was i.v. administered at three different dose levels to six cynomolgus monkeys on day 0. The graphs show changes in B-cell numbers in peripheral blood (panel A) and in lymph nodes (panel B) for different dose levels: 5 (circles), 25 (diamonds) and 50 mg/kg (squares). The symbols and error bars represent the mean and range of two different animals in each dose group.

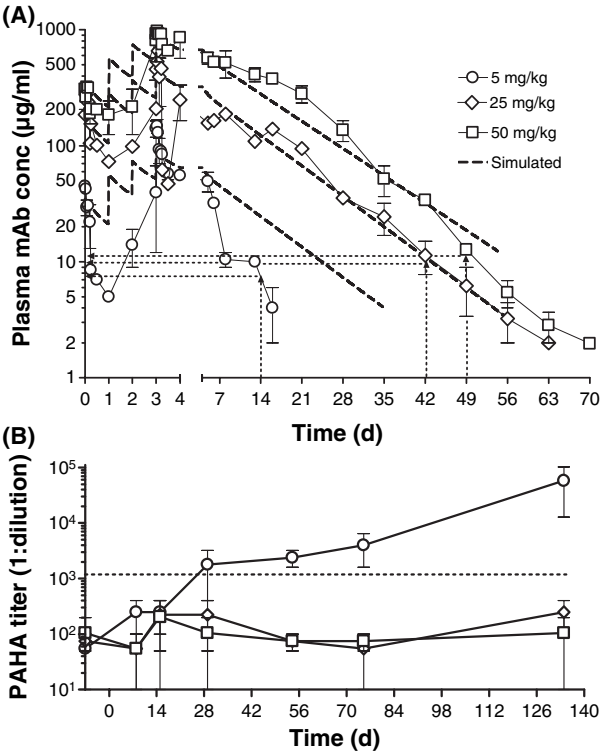

Fig 6. Pharmacokinetics of ofatumumab in monkeys. This figure relates to the same experiment as Fig 5. Panel A shows a semi-logarithmic plot of the plasma mAb concentrations observed in six cynomolgus monkeys after administration of ofatumumab at different dose levels of 1·25, 6·25 and 12·5 mg/kg, once daily as i.v. infusions (30 min) for four consecutive days, yielding total doses of 5 (circles), 25 (diamonds) and 50 mg/kg (squares), respectively. The symbols and error bars represent the mean and range for two monkeys. For comparison, the dashed lines give the expected concentrations at the three dose levels, based on simulations in a pharmacokinetic two-compartment model, applying a central distribution volume of 40 ml/kg and an elimination half-life of 9 d. Dotted arrows mark the time points at which the antibody treatment for B-cell depletion seemed to become ineffective (Fig 5) and the corresponding observed plasma concentrations. Panel B shows the development of primate-antihuman antibodies in the same monkeys (mean and range). The dotted line indicates the upper background level.

achitecture and cell composition in untreated animals, whereas germinal centre atrophy (mandibular and mesenteric) was observed in 67% (8/12) and 83% (10/12) of the lymph nodes obtained from animals receiving 20 mg/kg and 100 mg/kg, respectively.

Ofatumumab plasma concentrations following dosing at different dose levels are presented in a semi-logarithmic plot in Fig 6. To see whether distribution and clearance were as expected for IgG in monkeys, the observed data were compared to simulated curves obtained by using a two-compartment pharmacokinetic model. In these simulations, a central compartment volume (Vcen) of 40 ml/kg and an elimination half-life of 9 d were used, which match the values determined by Lin *et al* (1999) for a humanized mAb against VEGF in monkeys. The maximum concentrations observed shortly after completion of the series of four daily infusions were in accordance with the expected values. This indicates a normal distribution over plasma and interstitial compartments, without significant deviations because of target binding. The simulation clearly predicted the decay in plasma concentration after the high and medium doses. However, for the low-dosed monkeys, the observed values fell below the predicted values after 1 week. This rapid decay after low dosing corresponded to the occurrence of detectable levels of PAHA in these monkeys. Notably, in the high- and medium-dose monkeys, PAHA titres remained at pre-infusion levels, even at day 132 when ofatumumab concentrations in the plasma were far below detectable levels (Fig 6B).

Ofatumumab plasma concentrations above 50 µg/ml were shown to be sufficient for complete B-cell depletion (Figs 5 and 6). Furthermore, recovery of $CD20^+$ cells in peripheral blood and lymph nodes started when the ofatumumab concentration fell below about 5–10 µg/ml.

Discussion

In this present study, we showed that induction of ADCC and of CDC by ofatumumab *in vitro* each have their own concentration–effect relationship, with ADCC being active at lower antibody-binding levels than CDC. It can be anticipated that the dissociation of these two relationships will be different for different cell types, and may, amongst others, depend on the surface expression levels of CD20, complement defence molecules and molecules regulating cellular cytotoxicity. In contrast, however, little difference is to be expected in the position of the binding curve for different cell types. Importantly, saturation of CD20 binding occurred at a concentration of about 5 μg/ml, while maximum cytotoxic effects were reached at or below this concentration. Therefore, increasing mAb dose levels above the point of target saturation is not expected to increase the therapeutic effect. The present study evaluated this concept *in vivo* by estimating the minimum ofatumumab plasma concentration required for arresting tumour growth or the induction of maximum B-cell depletion.

In a mouse xenograft model with disseminated growth of a human B-cell line, antitumour effects were observed to be already maximal at the lowest dose (0·5 mg/kg) applied, which was estimated to give peak plasma concentrations of approximately 5 μg/ml. To determine the minimal effective plasma concentration, we examined the antibody concentration at which accelerated tumour growth occurred. This concentration was estimated to be around 0·5 μg/ml. Although we have no direct measurements of CD20 occupancy by ofatumumab on Daudi-luc cells in this model, it seems clear that ofatumumab maintained biological activity at concentrations that will give, at most, 50% saturation of the target.

The same approach was followed in analysing the ofatumumab dose requirements for depletion of circulating and resident B-cells in monkeys. The lowest total dose applied (5 mg/kg), yielding initial plasma concentrations of approximately 50 μg/ml, induced complete depletion of B cells from the peripheral blood. However, the observed PAHA formation in animals from this dose group indicated that an antibody response could still occur, suggesting that B cells were incompletely eliminated from the body. At higher dose levels, resulting in plasma concentrations above 100 μg/ml, depletion of all B cells was induced as confirmed by microscopic observations on lymph nodes and absence of PAHA responses. After a dose of 25 mg/kg, no PAHA were detectable in ELISA, not even on day 140, after complete disappearance of all ofatumumab from plasma. We also did not observe an accelerated plasma clearance that could indicate PAHA formation. After B-cell depletion in this experiment, recurrence of peripheral B cells was observed when plasma concentrations fell below 5–10 μg/ml. Thus, the minimal effective plasma concentration for maintaining peripheral B-cell depletion is expected to be between 5 and 10 μg/ml.

While both ADCC and CDC may be relevant for *in vivo* efficacy of ofatumumab, it is unclear which mechanism predominated in each of the evaluated animal models. Controversy exists on the *in vivo* mechanisms of action of the chimaeric anti-CD20 mAb, rituximab. Some studies in mouse models have shown a crucial role for FcγR (Clynes *et al*, 2000), whereas other mouse studies indicated that all activities depend on the complement system (Di Gaetano *et al*, 2003; Golay *et al*, 2006). Gong *et al* (2005) found evidence that the micro-environment of the target cells plays a critical role in the mechanism of action by rituximab. They showed in human CD20-transgenic mice that circulating B cells are rapidly cleared through effector cells of the reticuloendothelial system, whereas killing of B cells in peripheral compartments depended rather on complement-mediated than on Fc-receptor-mediated mechanisms. Apparently, both FcγR- and complement-dependent mechanisms may indeed play a role in the *in vivo* effects of anti-CD20 mAb, and it depends on the local conditions of the targeted cells which mechanism predominates. Because maximal engagement of ADCC and CDC occur at different levels of target saturation, this may explain the different dose requirements in the two models in our study. ADCC is likely to represent the main effector mechanism in our mouse model, because induction already occurred at relatively low target occupancy. In our monkey model, maintenance of B-cell depletion required higher ofatumumab plasma concentrations, indicating that ADCC may not be sufficient for depletion and complement activation may also be required.

Our studies revealed that the pharmacokinetics of ofatumumab may be affected by target binding. In the monkey studies, plasma concentrations in the first days after the 50 mg/kg dose were compatible with a distribution over the plasma compartment and interstitial space as described for IgG (Waldmann & Strober, 1969). However, at the lower dose levels, the concentrations in the first days were below those expected. Also, in the mouse model, we observed lower-than-expected plasma concentrations when ofatumumab was administered at a later stage of tumour development. This is consistent with observations in clinical trials. In a clinical trial with ofatumumab (HuMax-CD20) in patients with relapsed or refractory chronic lymphocytic leukaemia (B-CLL), ofatumumab was given at different dose levels, with weekly follow-up infusions (Coiffier *et al*, 2005). In this study, a rapid and variable plasma clearance was observed, which, in most patients, slowed on subsequent infusions (unpublished observations). Maloney *et al* (1994) also observed short serum half-lives (average of 4·4 d) in patients with relapsed non-Hodgkin lymphoma (NHL) receiving single infusions of rituximab. Also, in a clinical trial with NHL patients receiving four once-weekly rituximab dosing, the clearance rate was found to decrease on subsequent infusions and higher serum rituximab levels were observed in patients with an objective response to therapy (Berinstein *et al*, 1998). These clinical observations indicate that plasma clearance of anti-CD20 antibodies may be strongly affected by the presence of CD20-expressing tumour cells.

Previously, we studied plasma-to-tissue concentration gradients for a therapeutic antibody targeting the Epidermal Growth Factor receptor (Lammerts van Bueren *et al*, 2006). We found evidence that internalization and degradation of a therapeutic antibody after binding to a membrane target may create a significant 'sink' that accelerates clearance and lowers local concentrations in a tumour. Because CD20 has been characterized to be a non-internalizing membrane target (Press *et al*, 1989; Sieber *et al*, 2003), the rapid decay of anti-CD20 antibody concentration in patients is probably based on a gradually occurring saturation of the extra-vascular binding compartment consisting of CD20-expressing leukemic cells. It is, therefore, expected that once a binding equilibrium is established, there will be no local sink that will cause continued accelerated clearance. In addition, the binding compartment will be reduced when the treatment becomes effective.

We conclude from our study that ofatumumab plasma concentrations of 5–10 μg/ml are sufficient for ensuring sustained activity *in vivo*. This ofatumumab concentration is expected to be sufficient to saturate and induce maximal killing of circulating B cells. However, the monkey study clearly indicates that much higher ofatumumab plasma concentrations may be required to target CD20-expressing cells resident in the tissues in the initial phase of treatment. This seems highly relevant for designing the maintenance therapy regimens with ofatumumab. Recently, it has been shown by several investigators that, in follicular lymphoma, rituximab maintenance therapy gave significant prolongation of the response duration and improvement of survival (Hiddemann *et al*, 2006; van Oers *et al*, 2006). However, dosing schedules were empirically established and questions remain about the most effective dosing schedule in this application (Berinstein *et al*, 1998; Gordan *et al*, 2005). Our study supports the idea that, once the tumour mass is saturated with antibody and/or reduced in mass, relatively low plasma concentrations of ofatumumab will be sufficient to maintain optimal maintenance therapy.

References

Berinstein, N.L., Grillo-Lopez, A.J., White, C.A., Bence-Bruckler, I., Maloney, D., Czuczman, M., Green, D., Rosenberg, J., McLaughlin, P. & Shen, D. (1998) Association of serum Rituximab (IDEC-C2B8) concentration and anti-tumor response in the treatment of recurrent low-grade or follicular non-Hodgkin's lymphoma. *Annals of Oncology*, **9,** 995–1001.

Bleeker, W.K., Teeling, J.L. & Hack, C.E. (2001) Accelerated autoantibody clearance by intravenous immunoglobulin therapy: studies in experimental models to determine the magnitude and time course of the effect. *Blood*, **98,** 3136–3142.

Carter, P.J. (2006) Potent antibody therapeutics by design. *Nature Reviews of Immunology*, **6,** 343–357.

Clynes, R.A., Towers, T.L., Presta, L.G. & Ravetch, J.V. (2000) Inhibitory Fc receptors modulate *in vivo* cytoxicity against tumor targets. *Nature Medicine*, **6,** 443–446.

Coiffier, B., Tilly, H., Pedersen, L.M., Plesner, T., Frederiksen, H., van Oers, M.H.J., Wooldridge, J., Kloczko, J., Holowiecki, J., Hellmann, A., Walewski, J.J., Flensburg, M.F., Petersen, J. & Robak, T. (2005) HuMax CD20 fully human monoclonal antibody in chronic lymphocytic leuchemia. Early results from an ongoing Phase I/II Clinical Trial. *Blood (ASH Annual Meeting Abstracts)*, **106,** 448.

Cragg, M.S. & Glennie, M.J. (2004) Antibody specificity controls *in vivo* effector mechanisms of anti-CD20 reagents. *Blood*, **103,** 2738–2743.

De Vita, S. & Quartuccio, L. (2006) Treatment of rheumatoid arthritis with rituximab: an update and possible indications. *Autoimmunity Reviews*, **5,** 443–448.

Di Gaetano, N., Cittera, E., Nota, R., Vecchi, A., Grieco, V., Scanziani, E., Botto, M., Introna, M. & Golay, J. (2003) Complement activation determines the therapeutic activity of rituximab *in vivo*. *Journal of Immunology*, **171,** 1581–1587.

Fishwild, D.M., O'Donnell, S.L., Bengoechea, T., Hudson, D.V., Harding, F., Bernhard, S.L., Jones, D., Kay, R.M., Higgins, K.M., Schramm, S.R. & Lonberg, N. (1996) High-avidity human IgG kappa monoclonal antibodies from a novel strain of minilocus transgenic mice. *Nature Biotechnology*, **14,** 845–851.

Glennie, M.J. (2000) Signalling antibodies for the treatment of neoplastic disease. *Disease Markers*, **16,** 63.

Glennie, M.J. & van de Winkel, J.G. (2003) Renaissance of cancer therapeutic antibodies. *Drug Discovery Today*, **8,** 503–510.

Golay, J., Cittera, E., Di Gaetano, N., Manganini, M., Mosca, M., Nebuloni, M., van Rooijen, N., Vago, L. & Introna, M. (2006) The role of complement in the therapeutic activity of rituximab in a murine B lymphoma model homing in lymph nodes. *Haematologica*, **91,** 176–183.

Gong, Q., Ou, Q., Ye, S., Lee, W.P., Cornelius, J., Diehl, L., Lin, W.Y., Hu, Z., Lu, Y., Chen, Y., Wu, Y., Meng, Y.G., Gribling, P., Lin, Z., Nguyen, K., Tran, T., Zhang, Y., Rosen, H., Martin, F. & Chan, A.C. (2005) Importance of cellular microenvironment and circulatory dynamics in B cell immunotherapy. *Journal of Immunology*, **174,** 817–826.

Gordan, L.N., Grow, W.B., Pusateri, A., Douglas, V., Mendenhall, N.P. & Lynch, J.W. (2005) Phase II trial of individualized rituximab dosing for patients with CD20-positive lymphoproliferative disorders. *Journal of Clinical Oncology*, **23,** 1096–1102.

Grillo-Lopez, A.J., White, C.A., Dallaire, B.K., Varns, C.L., Shen, C.D., Wei, A., Leonard, J.E., McClure, A., Weaver, R., Cairelli, S. & Rosenberg, J. (2000) Rituximab: the first monoclonal antibody approved for the treatment of lymphoma. *Current Pharmaceutical Biotechnology*, **1,** 1–9.

Hiddemann, W., Buske, C., Dreyling, M., Weigert, O., Lenz, G. & Unterhalt, M. (2006) Current management of follicular lymphomas. *British Journal of Haematology*, **00,** 00.

Lammerts van Bueren, J.J., Bleeker, W.K., Bogh, H.O., Houtkamp, M., Schuurman, J., van de Winkel, J.G. & Parren, P.W. (2006) Effect of target dynamics on pharmacokinetics of a novel therapeutic antibody against the epidermal growth factor receptor: implications for the mechanisms of action. *Cancer Research*, **66,** 7630–7638.

Lin, Y.S., Nguyen, C., Mendoza, J.L., Escandon, E., Fei, D., Meng, Y.G. & Modi, N.B. (1999) Preclinical pharmacokinetics, interspecies scaling, and tissue distribution of a humanized monoclonal antibody against vascular endothelial growth factor. *Journal of Pharmacology and Experimental Therapeutics*, **288,** 371–378.

Maloney, D.G., Liles, T.M., Czerwinski, D.K., Waldichuk, C., Rosenberg, J., Grillo-Lopez, A. & Levy, R. (1994) Phase I clinical trial using escalating single-dose infusion of chimeric anti-CD20 monoclonal

antibody (IDEC-C2B8) in patients with recurrent B-cell lymphoma. *Blood*, **84,** 2457–2466.

van Oers, M.H., Klasa, R., Marcus, R.E., Wolf, M., Kimby, E., Gascoyne, R.D., Jack, A., Van't Veer, M., Vranovsky, A., Holte, H., van Glabbeke, M., Teodorovic, I., Rozewicz, C. & Hagenbeek, A. (2006) Rituximab maintenance improves clinical outcome of relapsed/resistant follicular non-Hodgkin lymphoma in patients both with and without rituximab during induction: results of a prospective randomized phase 3 intergroup trial. *Blood*, **108,** 3295–3301.

Press, O.W., Farr, A.G., Borroz, K.I., Anderson, S.K. & Martin, P.J. (1989) Endocytosis and degradation of monoclonal antibodies targeting human B-cell malignancies. *Cancer Research*, **49,** 4906–4912.

Sell, S. & Fahey, J.L. (1964) Relationship between gamma-globulin metabolism and low serum gamma-globulin in germfree mice. *Journal of Immunology*, **93,** 81–87.

Sieber, T., Schoeler, D., Ringel, F., Pascu, M. & Schriever, F. (2003) Selective internalization of monoclonal antibodies by B-cell chronic lymphocytic leukaemia cells. *British Journal of Haematology*, **121,** 458–461.

Teeling, J.L., French, R.R., Cragg, M.S., Van Den Brakel, J., Pluyter, M., Huang, H., Chan, C., Parren, P.W., Hack, C.E., Dechant, M., Valerius, T., Van De Winkel, J.G. & Glennie, M.J. (2004) Characterization of new human CD20 monoclonal antibodies with potent cytolytic activity against non-Hodgkin lymphomas. *Blood*, **104,** 1793–1800.

Teeling, J.L., Mackus, W.J., Wiegman, L.J., van den Brakel, J.H., Beers, S.A., French, R.R., van Meerten, T., Ebeling, S., Vink, T., Slootstra, J.W., Parren, P.W., Glennie, M.J. & van de Winkel, J.G. (2006) The biological activity of human CD20 monoclonal antibodies is linked to unique epitopes on CD20. *Journal of Immunology*, **177,** 362–371.

Vugmeyster, Y., Howell, K., McKeever, K., Combs, D. & Canova-Davis, E. (2003) Differential *in vivo* effects of rituximab on two B-cell subsets in cynomolgus monkeys. *International Immunopharmacology*, **3,** 1477–1481.

Waldmann, T.A. & Strober, W. (1969) Metabolism of immunoglobulins. *Progress in Allergy*, **13,** 1–110.